

Article

On-Board State-of-Health Estimation at a Wide Ambient Temperature Range in Lithium-Ion Batteries

Tiansi Wang, Lei Pei *, Tingting Wang, Rengui Lu and Chunbo Zhu *

School of Electrical Engineering and Automation, Harbin Institute of Technology, Harbin 150001, China; E-Mails: tiansi.wang@hotmail.com (T.W.); wuyu2012331@163.com (T.W.); lurengui@hit.edu.cn (R.L.)

* Authors to whom correspondence should be addressed; E-Mails: lei.pei@hotmail.com (L.P.); zhuchunbo@hit.edu.cn (C.Z.); Tel./Fax: +86-451-8641-3621 (L.P. & C.Z.).

Academic Editor: Haolin Tang

Received: 18 June 2015 / Accepted: 3 August 2015 / Published: 11 August 2015

Abstract: A state-of-health (SOH) estimation method for electric vehicles (EVs) is presented with three main advantages: (1) it provides joint estimation of cell's aging states in terms of power and energy (*i.e.*, SOH_P and SOH_E)—because the determination of SOH_P and SOH_E can be reduced to the estimation of the ohmic resistance increase and capacity loss, respectively, the ohmic resistance at nominal temperature will be taken as a health indicator, and the capacity loss is estimated based on a mechanistic model that is developed to describe the correlation between resistance increase and capacity loss; (2) it has wide applicability to various ambient temperatures—to eliminate the effects of temperature on the resistance, another mechanistic model about the resistance against temperature is presented, which can normalize the resistance at various temperatures to its standard value at the nominal temperature; and (3) it needs low computational efforts for on-board application—based on a linear equation of cell's dynamic behaviors, the recursive least-squares (RLS) algorithm is used for the resistance estimation. Based on the designed performance and validation experiments, respectively, the coefficients of the models are determined and the accuracy of the proposed method is verified. The results at different aging states and temperatures show good accuracy and reliability.

Keywords: lithium-ion batteries; state-of-health (SOH); wide temperature range; resistance increase; capacity loss

1. Introduction

The usage of lithium-ion batteries as a storage system is currently the best choice for portable applications, such as electric vehicles (EVs) and mobile electronics, based on comprehensive consideration of its energy and power density and cycle-life [1]. Unfortunately, with battery aging, its maximum available energy and instantaneous power will gradually fade. In this paper, we will focus on developing an effective estimation technology of the state-of-health (SOH) for lithium-ion batteries in EVs such as battery electric vehicles (BEVs) and hybrid electric vehicles (HEVs).

For EVs, battery SOH is always defined with two specific forms, and they are SOH_E and SOH_P to indicate the degradation of energy and power, respectively. Based on the simplification processes shown in Equations (1) and (2), respectively, the determination of the battery SOH_E and SOH_P can be reduced to the estimation of the capacity and ohmic resistance [2]. Wherein, U_{bat} and I_{bat} indicate the terminal voltage and the load current, respectively; C_{bat} , open-circuit voltage (OCV), and R_o indicate the capacity, open-circuit voltage, and ohmic resistance, respectively; subscripts “a” and “0” indicate the aging value and initial value of the marked variables, respectively:

$$SOH_E = \frac{Energy_a}{Energy_0} = \frac{\int_0^{t_a} U_{bat,t} I_{bat,t} dt}{\int_0^{t_0} U_{bat,t} I_{bat,t} dt} \approx \frac{(U_{bat,max} - U_{bat,min}) C_{bat,a}}{(U_{bat,max} - U_{bat,min}) C_{bat,0}} = \frac{C_{bat,a}}{C_{bat,0}} \times 100\% \quad (1)$$

$$SOH_P = \frac{Power_a}{Power_0} \approx \frac{U_{bat,min} (OCV - U_{bat,min}) / R_{o,a}}{U_{bat,min} (OCV - U_{bat,min}) / R_{o,0}} = \frac{R_{o,0}}{R_{o,a}} \times 100\% \quad (2)$$

For internal resistance identification, the most basic methods are performed by fitting the measured data of the hybrid pulse power characteristic (HPPC) tests or the electrochemical impedance spectroscopy (EIS) tests in least-squares sense under off-line operation conditions [3,4]. In addition, the results of these off-line identifications are always taken as reference values for on-line methods or training data for battery modelling. For the on-line methods, the resistances are always estimated on the basis of equivalent circuit models (ECMs) [5–10] or electrochemical models [11–13] with the utilization of the recursive optimal estimation algorithms, such as the Kalman-filter-based algorithms and the least-squares-based algorithms.

Compared with the resistance identification, the battery capacity cannot be directly identified and will always be calculated by some specific health indicators. In [14–16], the OCV of $LiCO_2$ is selected as the health indicator, and the battery capacity is estimated by a ratio between the changes of coulomb counting and the corresponding changes of state-of-charge (SOC), which is determined by the predefined OCV-SOC relation. However, in most cases, the OCV-SOC relations are not steep enough and always change with aging. For example, the OCV of $LiFePO_4$ cell shows a flat plateau over a large SOC range due to the two-phase reaction process and the shape of the OCV profile changes obviously at the deep aging stage caused by active material loss. In [17–20], based on the analysis of OCV curve changes, the capacity of $LiFePO_4$ is calculated by an incremental capacity analysis (ICA) to the quasi-OCV curve that is obtained by a discharge process with a tiny current. Besides the OCV, some other parameters can also be used as the indicators. As introduced in [21], the diffusion capacitance of an ECM is taken as the indicator and a correlation between the diffusion capacitance and battery capacity is established.

For a joint estimation for SOH_P and SOH_E, the internal resistance can be taken as the health indicator, and the SOH_E will be estimated by establishing a correlation between the capacity loss and resistance increase [2]. However, the resistance values are very sensitive to temperature changes and the effects of temperature on the resistances are not sufficiently discussed in the existing methods. In addition, the correlation between the capacity loss and resistance increase always lacks of reasonable explanations in terms of chemical and physical meanings.

In this paper, a joint estimation method of SOH_P and SOH_E for EVs over a wide temperature range is proposed with a health indicator of battery ohmic resistance. In Section 2, two mechanistic models are established to describe the relationships for the resistance changes against temperatures and capacity loss, respectively, and a systematic estimation procedure is proposed. Based on the experiments designed in Section 3, the coefficients of the models are determined by fitting the data of characteristic experiments, and the accuracy of the new method is verified with the validation experiments in Section 4. Finally, conclusions are drawn in Section 5.

2. Models and Methods

2.1. The Relationship between Resistance Increase and Capacity Loss

In the aging stage of batteries used in EVs (*i.e.*, capacity loss <20%), the capacity loss (Q_{loss}) is mainly caused by the loss of lithium inventory with the formation and thickening of the solid electrolyte interphase (SEI) film [4,22], so the capacity loss will be accompanied by the SEI film resistance (R_{SEI}) increase.

As studied in [23,24], the SEI film mainly consists of two kinds of components: inorganic and organic substances. If the proportion of inorganic and organic substances within the new SEI film are marked by m and $(1 - m)$, and their resistances are marked as $R_{\text{SEI-M}}$ and $R_{\text{SEI-N}}$, respectively, the correlation between resistance increase and capacity loss can be described as Equation (3). Herein, $R_{\text{SEI-M}}$ and $R_{\text{SEI-N}}$ are proportional to respective capacity loss by default, respectively; the subscript “a” indicates the change caused by aging; and the proportional coefficients of a_M and a_N are the characteristic coefficients dependent on materials:

$$dR_{\text{SEI,a}} = dR_{\text{SEI-M,a}} + dR_{\text{SEI-N,a}} = a_M \times m dQ_{\text{loss}} + a_N \times (1 - m) dQ_{\text{loss}} \quad (3)$$

With the battery aging, the contents of two kinds of the components will change accordingly. On the one hand, with battery aging, SEI film continually grows from the graphite anode surface and its thickness accordingly increases [25,26]. On the other hand, for the SEI film, the dense inner layers close to the graphite are mainly composed of inorganic substances, and the porous outer layers close to the electrolyte mainly consist of organic substances [24,27]. That means, with the capacity loss due to SEI growth, the proportion of organic substances in the new forming SEI film gradually decreases and that of inorganic substances correspondingly increases. When we suppose m is proportional to Q_{loss} (*i.e.*, $m = bQ_{\text{loss}}$), as expressed in Equation (4), the correlation between the Q_{loss} and R_{SEI} can be obtained by integrating the Equation (3). Wherein, a_1 , a_2 and C are the unknown coefficients in derivation process:

$$\int dR_{SEI,a} = \int [a_M b Q_{loss} + a_N (1 - b Q_{loss})] dQ_{loss}$$

$$\Rightarrow R_{SEI,a} = a_1 Q_{loss}^2 + a_2 Q_{loss} + C \quad (4)$$

Because a part of SEI film has formed in prior formation cycles before the cells leave the factories, the current SEI film will contain two parts: an initial SEI layer (corresponding to $R_{SEI,0}$ and $Q_{loss,0}$) and a further growth SEI layer (corresponding to $\Delta R_{SEI,a}$ and ΔQ_{loss}). Thus, Equation (4) can be transformed to Equation (5):

$$(\Delta R_{SEI,a} + R_{SEI,0}) = a_1 (\Delta Q_{loss} + Q_{loss,0})^2 + a_2 (\Delta Q_{loss} + Q_{loss,0}) + C \quad (5)$$

Simplifying Equation (5), we can get the function correlation between the resistance increase and capacity loss as shown in Equation (6):

$$\Delta R_{SEI,a} = \alpha_1 \Delta Q_{loss}^2 + \alpha_2 \Delta Q_{loss} \quad (6)$$

However, the R_{SEI} cannot be independently identified and will be included in the on-line identification result of the R_o , which is always estimated using the online measured voltage and current data. According to the EIS analysis results presented in [28,29], the R_o mainly corresponds to the internal resistances relevant to fast electrochemical processes, containing the resistances of electrolyte/electrical transport in bulk phase (R_{bulk}), SEI film resistance (R_{SEI}), and the resistance of faradaic charge transfer at the electrode interphase (R_{ct}), and can be approximately expressed as Equation (7):

$$R_o = R_{bulk} + R_{SEI} + R_{ct} \quad (7)$$

Because R_{bulk} and R_{ct} nearly remain unchanged in this aging stage [28], it can be concluded that the increment of R_o is almost equal to that of R_{SEI} , as expressed in Equation (8):

$$\Delta R_{o,a} = \Delta R_{bulk,a} + \Delta R_{SEI,a} + \Delta R_{ct,a} \approx \Delta R_{SEI,a} \quad (8)$$

Based on the Equation (8), the function relationship of ΔQ_{loss} with respect to $\Delta R_{o,a}$, which is the inverse function of Equation (6), can be expressed by Equation (9). Wherein, the coefficients α_1 and α_2 will be determined by experimental data:

$$\Delta Q_{loss} = \frac{-\alpha_2 + \sqrt{\alpha_2^2 + 4\alpha_1 \Delta R_{SEI,a}}}{2\alpha_1} \approx \frac{-\alpha_2 + \sqrt{\alpha_2^2 + 4\alpha_1 \Delta R_{o,a}}}{2\alpha_1} \quad (9)$$

2.2. The Effects of Temperature on Internal Resistances

The effects of temperature on different kinds of internal resistances are different, so different internal resistances may have different changing trends. For the bulk and SEI resistance (*i.e.*, R_{bulk} and R_{SEI}), the resistance increment is a near linear function of temperature change; however, for the charge transfer resistance (*i.e.*, R_{ct}), the resistance value is inversely proportional to the electrochemical reaction rate and the reaction rate follows an Arrhenius dependence with temperature (T) [30]. Therefore, the correlation between the ohmic resistance change ($\Delta R_{o,t}$) and T can be deduced as Equation (10). Wherein, the subscript “ t ” indicates the change caused by “ t ” ambient temperatures;

the coefficients κ_1 – κ_4 will be determined by experimental data; and T_{std} indicates the nominal temperature which is set to 30 °C in this paper:

$$\begin{aligned} \Delta R_{o,t} &= \Delta R_{bulk,t} + \Delta R_{SEI,t} + \Delta R_{ct,t} \\ &= k_{bulk} (T - T_{std}) + k_{SEI-M} (T - T_{std}) + k_{SEI-N} (T - T_{std}) + k_{ct} \left(\frac{1}{e^{-E_a/(T+273)}} - \frac{1}{e^{-E_a/(T_{std}+273)}} \right) \\ &= \kappa_1 T + \kappa_2 e^{\kappa_3/(T+273)} + \kappa_4 \end{aligned} \tag{10}$$

This new mechanistic model can be used to eliminate the effects of temperatures on the ohmic resistance, which ensures that the SOH estimation can be used over a wide temperature range in practical operations.

2.3. The Parameter Identification Method

As shown in Figure 1, an ECM employing a resistance in series with a parallel resistance and capacitance (R-RC), which is proved to be the best choice for pursuing the balance between the fitting effects and the computational efforts and most widely applied for battery state estimations [31,32], is chosen for on-line resistance identification in this study. Wherein, the OCV is used to express the internal voltage source of the battery model; R_o and R_p denote the ohmic resistance and polarization resistance, respectively; and C_p is the polarization capacitance.

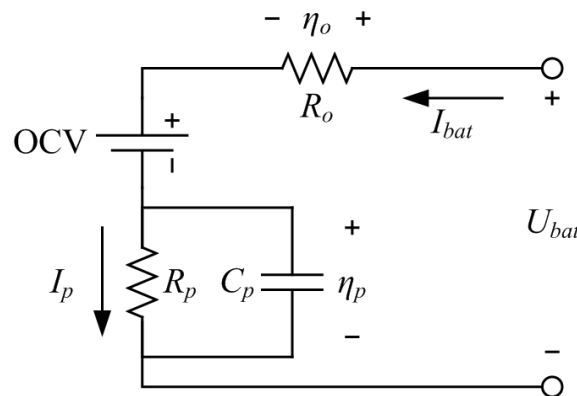


Figure 1. A resistance in series with a parallel resistance and capacitance (R-RC) model.

The on-line internal resistance identification method requires determination with two steps:

First, based on the chosen ECM, the terminal voltage of a cell can be expressed as Equation (11) [33]. Herein, the subscript “ k ” represents k th time step, and $\tau_p = R_p C_p$:

$$U_{bat,k-1} = OCV + (R_o + R_p) I_{bat,k-1} + R_o \tau_p \frac{I_{bat,k} - I_{bat,k-1}}{\Delta t} + \tau_p \frac{U_{bat,k-1} - U_{bat,k}}{\Delta t} \tag{11}$$

Separating the known and unknown variables of Equation (11) and rearrangement yield a linear expression about the parameter vector, as shown in Equation (12). Wherein, z_k and ϕ_k are obtained by the measured data of the current and voltage at the sample points; and $\theta_k = [OCV, R_{o,k} + R_{p,k}, R_{o,k} \tau_{p,k}, \tau_{p,k}]^T$ is the target vector to be determined:

$$\underbrace{U_{\text{bat},k-1}}_{z_k} = \underbrace{\begin{bmatrix} 1 & I_{\text{bat},k-1} & \frac{I_{\text{bat},k} - I_{\text{bat},k-1}}{\Delta t} & \frac{U_{\text{bat},k-1} - U_{\text{bat},k}}{\Delta t} \end{bmatrix}}_{\varphi_k^T} \underbrace{\begin{bmatrix} \text{OCV}_k & R_{o,k} + R_{p,k} & R_{o,k} \tau_{p,k} & \tau_{p,k} \end{bmatrix}}_{\theta_k}^T \quad (12)$$

Second, to identify the parameters in real time, a discrete-time filter is always needed. The recursive least-squares (RLS) algorithm with a forgetting factor is adopted in this study, which is very suitable for on-board applications due to its low computational efforts and memory consumptions. Refer to [34,35] for details of the RLS method and its generalization. The implementation of RLS algorithm with a forgetting factor is detailed in Table 1. Herein, P_k represents an estimation error covariance matrix; K_k indicates a gain matrix; and $\hat{\cdot}$ represents an estimation value.

Following the procedure in Table 1, the target vector θ_k can be easily determined, and the identification results of the parameters can be calculated as follows:

- (1) Initial the target vector θ_0 and the covariance matrix P_0 ;
- (2) For $k = 1, 2, 3, \dots$, after new measurements, z_k and φ_k are available;
- (3) Update θ_k and P_k with the equations in Table 1;
- (4) Calculate the parameter values with Equation (13).

$$\begin{cases} \text{OCV}_k = \theta_k(1) \\ R_{o,k} = \theta_k(3)/\theta_k(4) \\ R_{p,k} = \theta_k(2) - \theta_k(3)/\theta_k(4) \\ \tau_{p,k} = \theta_k(4) \end{cases} \quad (13)$$

Table 1. Procedures of the recursive least-squares (RLS) for parameter identification.

Initializations ^a	Updates ^b
$\hat{\theta}_0 = 0, P_0 = \delta^{-1}I$	$K_k = P_{k-1}\varphi_k / (\lambda + \varphi_k^T P_{k-1} \varphi_k)$ $\hat{\theta}_k = \hat{\theta}_{k-1} + K_k (z_k - \hat{\theta}_{k-1}^T \varphi_k)$ $P_k = (I - K_k \varphi_k^T) P_{k-1} / \lambda$

^a δ is set to 10^{-3} ; ^b λ is a forgetting factor.

2.4. State of Health (SOH) Estimation Procedure

Based on the new models and parameter identification method presented above, a new SOH estimation procedure is shown in Figure 2.

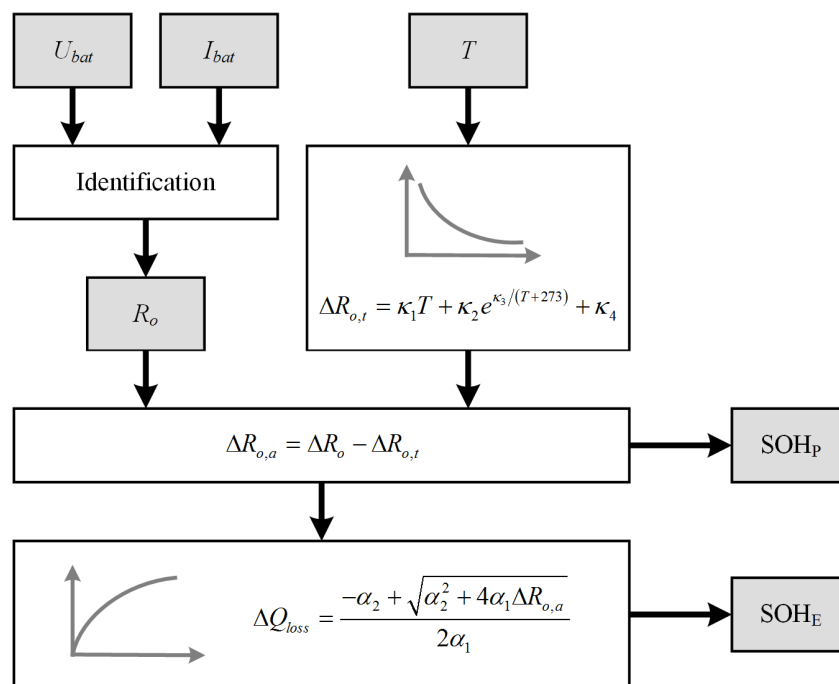


Figure 2. The procedure of the State of Health (SOH) estimation method.

The procedure is listed as follows: (1) on-line ohmic resistance identification: through the measurements of battery voltage and current, the ohmic resistance values can be identified on line using the RLS algorithm; (2) SOH_P estimation: according to the measured ambient temperature, the ohmic resistance increment caused by various temperatures can be calculated by Equation (10), and then this increment is subtracted from the identified resistance, which is a resistance normalization process, so the normalized resistance can be used to reflect battery aging levels and estimate SOH_P by Equation (2); (3) SOH_E estimation: the capacity loss can be obtained by substitution of the normalized R_o increment into Equation (9), and then the SOH_E can be calculated according to Equation (1).

3. Experiment Design

To determine the coefficients of the mechanistic models and verify the accuracy of the estimation method, the experiments are designed as follows.

3.1. Experiment Object

In this research, 32650-type LiFePO₄/graphite cells (OptimumNano Energy Co. Ltd., Shenzhen, China) with the nominal capacity of 5 Ah were chosen as the research objects, and the upper and lower limit voltages of the chosen cells are 3.65 V and 2.5 V, respectively.

3.2. Experiment Procedure

In this study, the experiments consist of two main parts: the aging cycles and the performance tests. In addition, the performance tests can be subdivided into the characteristic tests and the validation tests, as shown in Figure 3.

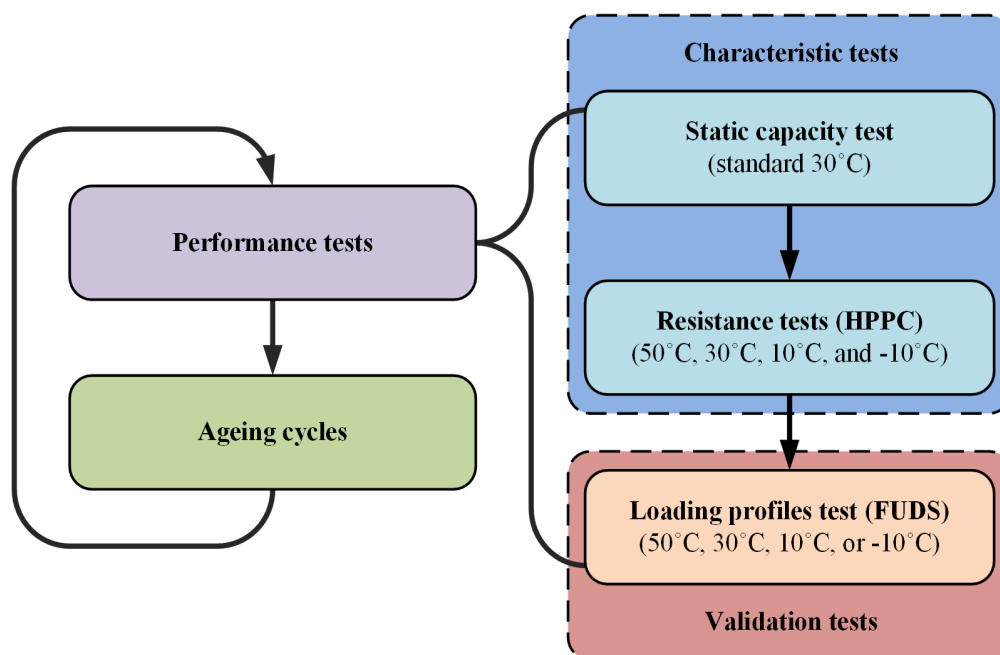


Figure 3. The procedure of experiments.

To shorten the period of the aging experiments, the aging cycles were performed at the ambient temperature of 60 °C with the current of 1 C-rate. The performance tests were performed every 100 aging cycles, which contain three parts: a static capacity test, an internal resistance test, and a validation test. Herein, the capacity test was performed with a CC-CV (constant current-constant voltage) charge and a constant discharge with the current of 1 C-rate at a normal temperature of 30 °C; the HPPC tests, as the resistance tests, were conducted at four different temperatures (in the order of 50 °C, 30 °C, 10 °C, and −10 °C); and Federal Urban Driving Schedule (FUDS) tests taken as validation experiments were performed at set temperatures of 50 °C, 30 °C, 10 °C, and −10 °C, respectively.

3.3. Experiment Equipment

All the tests were performed with a channel of the Arbin instruments' BT2000 test bench (Arbin Instruments Co. Ltd., College Station, TX, USA), which has a voltage measurement accuracy of $\pm 0.01\%$ and a current measurement accuracy of $\pm 0.02\%$ on the full-scale value of both ranges (18 V, ± 10 A for the medium current range and ± 100 A for the high current range). Moreover, the cell ambient temperatures were controlled within ± 2 °C by incubators in all tests.

4. Results and Discussion

4.1. Performance Test Results

The capacity values of the battery obtained by the static capacity tests are shown as follows in Table 2.

Table 2. Cell capacity and capacity loss at different aging states.

Aging state	Capacity (Ah)	Q_{loss} (Ah)
Fresh	4.992	0
100 cycles	4.762	0.23
200 cycles	4.378	0.614
300 cycles	3.754	1.238

The reference values of ohmic resistance are identified with the least-squares method applied to the voltage and current data from the pulse current experiments of HPPC tests, and the results at different aging levels and temperatures are shown in Figure 4. For brevity, the application process of the least-squares fit is omitted here.

From Figure 4, it can be observed that the R_o values increase with the battery aging and are nearly identical in the SOC range from 0.4 to 0.6. Thus, the R_o values at around SOC = 0.5 are taken as the indicators. This selection not only ensures the resistance values are hardly affected by the SOC estimation errors at an acceptable level (e.g., less than $\pm 5\%$) but also makes it possible to implement the algorithm in different types of EVs (e.g., general SOC ranges of 0.2–1 for BEVs and 0.3–0.7 for HEVs).

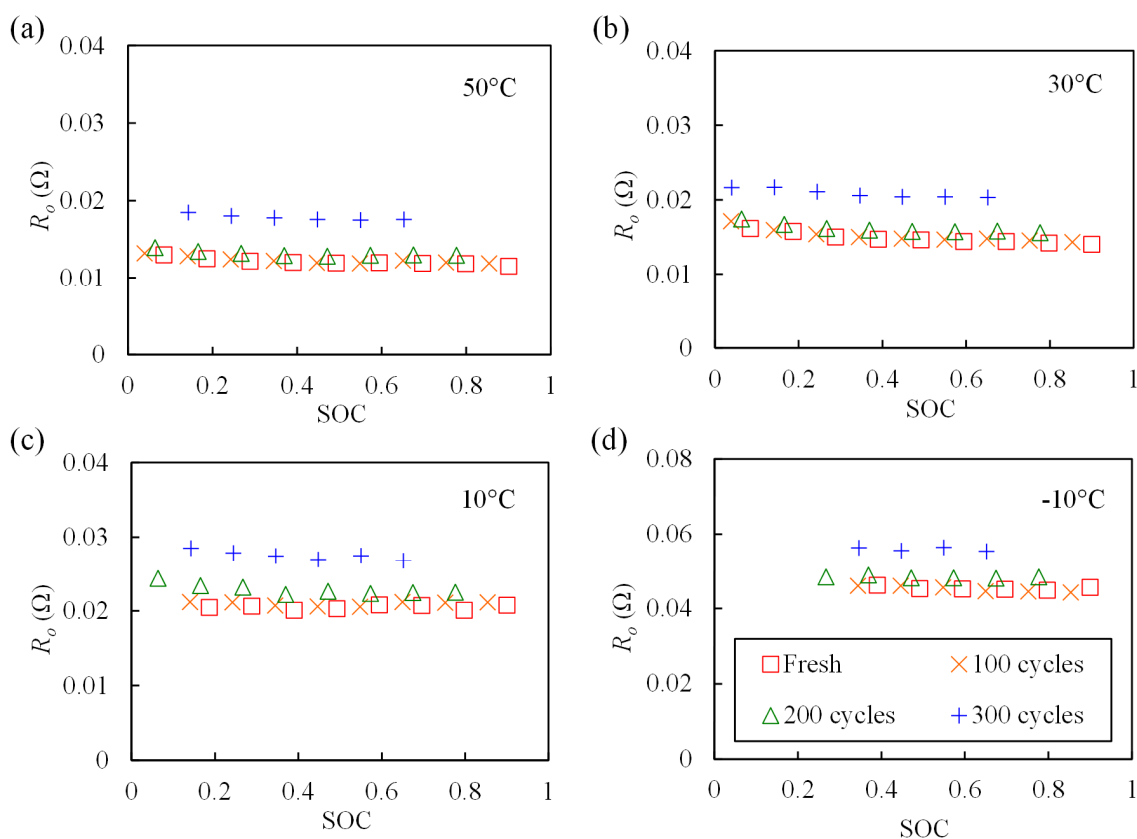


Figure 4. R_o values of different aging cycles at various temperatures: (a) 50 °C; (b) 30 °C; (c) 10 °C; (d) –10 °C.

The values of R_o at around SOC = 0.5 are plotted against different temperatures and aging states in Figure 5. From this figure, it can be observed that R_o increases with battery ages and temperature decreases. To verify the reliability of the mechanistic models and determine the coefficients of the

proposed models, the specific correlations of R_o increment with respect to capacity loss ($\Delta R_{o,a}$ vs. Q_{loss}) and temperature ($\Delta R_{o,t}$ vs. T) will be further investigated in the next subsection.

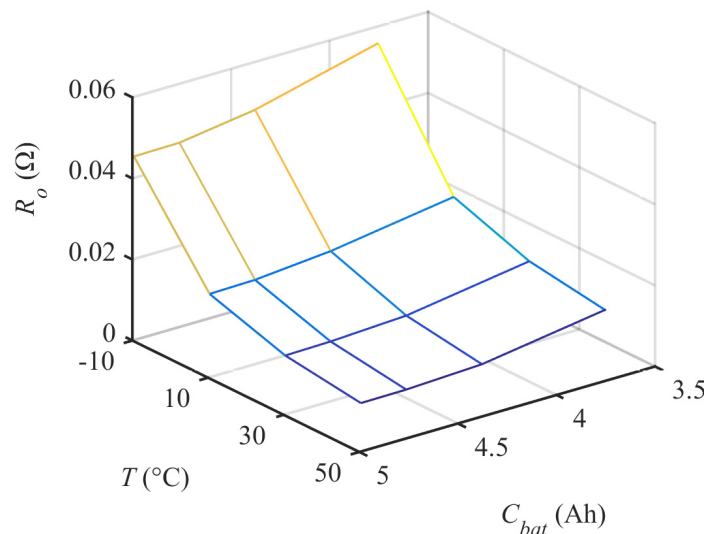


Figure 5. R_o values with different temperatures at different aging levels.

4.2. Model Coefficient Determining

First, as a part of Figure 5, the capacity loss is plotted against resistance increase at the nominal temperature by discrete points in Figure 6. Based on these discrete data, the coefficients of Equation (9) are fitted with the least-squares method and the fitting results are given as Equation (14):

$$\Delta Q_{loss} = \frac{-\alpha_2 + \sqrt{\alpha_2^2 + 4\alpha_1 \Delta R_{o,a}}}{2\alpha_1}, \text{ where } \begin{cases} \alpha_1 = 4.154 \times 10^{-3} \\ \alpha_2 = 2.623 \times 10^{-4} \end{cases} \quad (14)$$

Additionally, the fitted curve is also plotted in Figure 6. From the fitting results, it can be observed that the experiment results are highly consistent with the predictions of the mechanistic model for the relation between capacity loss and resistance increase (*i.e.*, Equation (9)). Wherein, the small fitting errors are probably caused by the simplification to the complex components of SEI film.

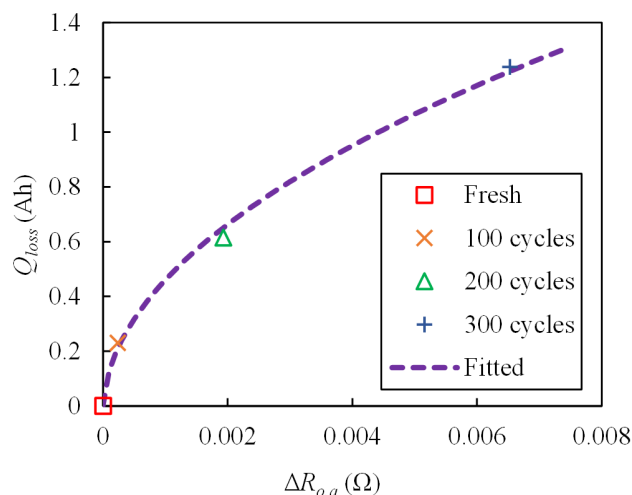


Figure 6. The relationship between $\Delta R_{o,a}$ and Q_{loss} .

Second, the relationship between the ohmic resistance increment (relative to the nominal value at 30 °C) and temperature is plotted in Figure 7 with discrete points.

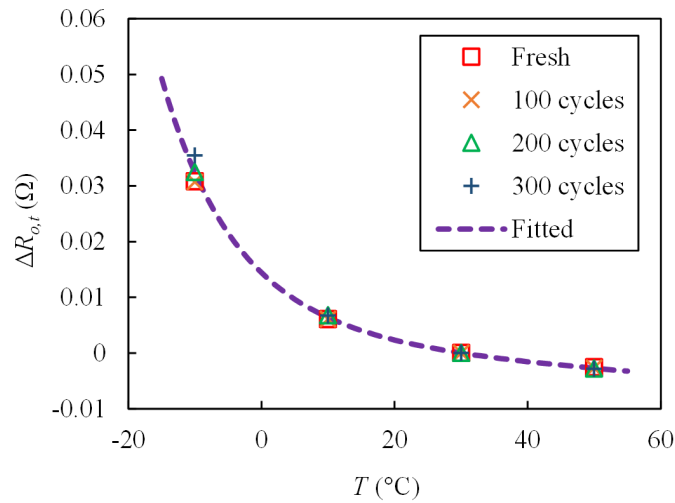


Figure 7. The relationship of $\Delta R_{o,t}$ with temperature.

The unknown coefficients of Equation (10) are determined by a least-squares fit of these discrete data, and the results are shown as Equation (15). The fitted curve is also plotted in Figure 7 and shows that the incremental changes in ohmic resistance along temperatures follow an exponential relationship, which agrees well with the predictions of the mechanistic model reflecting the temperature effects.

$$\Delta R_{o,t} = \kappa_1 T + \kappa_2 e^{\kappa_3/(T+273)} + \kappa_4, \text{ where } \begin{cases} \kappa_1 = 7.602 \times 10^{-12} \\ \kappa_2 = 5.818 \times 10^3 \\ \kappa_3 = 2.236 \times 10^{-2} \\ \kappa_4 = -7.928 \times 10^{-5} \end{cases} \quad (15)$$

4.3. Validating Results

In consideration of the effects of ambient temperatures on the estimation algorithm, the FUDS working condition experiments, which were performed on the cells under four different conditions of fresh state/50 °C, 100 aging cycles/30 °C, 200 aging cycles/10 °C, and 300 aging cycles/−10 °C, are chosen to verify the estimation accuracy of the algorithm. Based on the collected data of terminal voltage and load current, the ohmic resistance is identified by applying the RLS algorithm with a forgetting factor to Equation (12) with the initial values of $\theta_0 = [0 \ 0 \ 0 \ 0]^T$ and the forgetting factor $\lambda = 0.999$. The identified results are shown by solid curves in Figure 8, and compared with the reference values obtained from off-line HPPC tests.

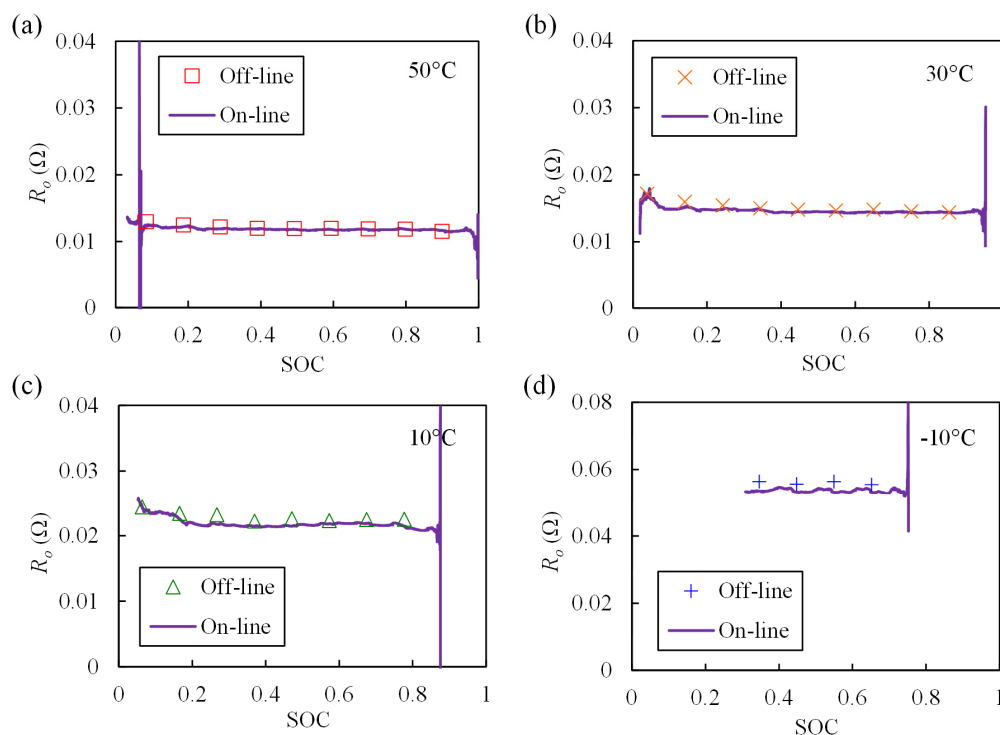


Figure 8. The comparison of the identification and reference values of R_o : (a) fresh values at 50 °C; (b) the values after 100 cycles at 30 °C; (c) the values after 200 cycles at 10 °C; (d) the values after 300 cycles at −10 °C.

From Figure 8, it can be found that there are only small differences between the identified results and the reference values in all four tests, suggesting a good robustness of the identification method at different temperatures and aging levels. Wherein, the estimated R_o values are always slightly less than the reference values of the HPPC tests, probably because the cell's inner temperature will be slightly higher than the ambient temperature under continuous operation conditions, especially for a lower ambient temperature.

Based on the ohmic resistance identification results, the SOH_P and SOH_E estimation results are obtained by following the procedure presented in Section 2.4, and are shown in Table 3. Table 3 shows that the on-line SOH_P and SOH_E estimation errors of the new method are less than $\pm 5\%$ at various ambient temperatures and aging states, which indicates that the proposed approach has good accuracy and reliability for on-board application.

Table 3. Validation results for state-of-health (SOH_P and SOH_E).

Aging cycles	Temperature (°C)	Measured SOH_P (%)	Estimated SOH_P (%)	Measured SOH_E (%)	Estimated SOH_E (%)
0	50	100.0	100.6	100.0	100.6
100	30	98.4	99.8	95.4	98.7
200	10	92.2	94.7	87.7	91.8
300	−10	71.3	70.9	75.2	76.7

5. Conclusions

This paper proposes an on-line SOH estimation method for lithium-ion batteries applied in EVs. The presented SOH estimation method has three characteristics: (1) joint estimation of SOH_P and

SOH_E; (2) eliminating ambient temperature effects; and (3) low computational efforts for on-board application. In this study, the establishment of two mechanistic models is confirmed to be reliable and accurate by the battery characteristic tests, and the coefficients of the models are determined by a curve fit. Additionally, the proposed method has been verified by the validation experiments, and the results show good accuracy and wide applicability at various ambient temperatures.

Acknowledgments

This research was supported in part by an International Cooperation and Exchange Program between the National Natural Science Funds of China and the UK Engineering and Physical Sciences Research Council (NSFC: 51361130153, EPSRC: EP/L001063/1), in part by the Research and Development of Application Technology Plan Project in Heilongjiang Province of China (GA13A202), and in part by the Science and Technology Project of the State Grid Corporation of China. The author would also like to thank the reviewers for their corrections and helpful suggestions.

Author Contributions

Tiansi Wang and Lei Pei cooperated to develop the new method and complete the main parts of the manuscript. Tingting Wang was involved in battery modelling. Rengui Lu and Chunbo Zhu gave some suggestions for the preparation of the manuscript.

Conflicts of Interest

The authors declare no conflict of interest.

Abbreviations

BEV	battery electric vehicle
ECM	equivalent circuit model
EIS	electrochemical impedance spectroscopy
EV	electric vehicle
FUDS	Federal Urban Driving Schedule
HEV	hybrid electric vehicle
HPPC	hybrid pulse power characterization
ICA	incremental capacity analysis
RLS	recursive least-squares
R-RC	a resistance in series with a parallel resistance and capacitance
SEI	solid electrolyte interphase
SOC	state-of-charge
SOH	state-of-health

References

1. Scrosati, B.; Garche, J. Lithium batteries: Status, prospects and future. *J. Power Sources* **2010**, *195*, 2419–2430.

2. Waag, W.; Fleischer, C.; Sauer, D.U. Critical review of the methods for monitoring of lithium-ion batteries in electric and hybrid vehicles. *J. Power Sources* **2014**, *258*, 321–339.
3. *PNGV Battery Test Manual: Revision 3*; Technical Report for US Department of Energy: Washington, DC, USA, 2001.
4. Eddahech, A.; Briat, O.; Bertrand, N.; Delétage, J.Y.; Vinassa, J.M. Behavior and state-of-health monitoring of Li-ion batteries using impedance spectroscopy and recurrent neural networks. *Int. J. Electr. Power Energy Syst.* **2012**, *42*, 487–494.
5. Plett, G.L. Extended kalman filtering for battery management systems of lipb-based hev battery packs: Part 3. State and parameter estimation. *J. Power Sources* **2004**, *134*, 277–292.
6. He, H.; Xiong, R.; Guo, H. Online estimation of model parameters and state-of-charge of LiFePO₄ batteries in electric vehicles. *Appl. Energy* **2012**, *89*, 413–420.
7. Pei, L.; Zhu, C.; Wang, T.; Lu, R.; Chan, C.C. Online peak power prediction based on a parameter and state estimator for lithium-ion batteries in electric vehicles. *Energy* **2014**, *66*, 766–778.
8. Roscher, M.A.; Bohlen, O.S.; Sauer, D.U. Reliable state estimation of multicell lithium-ion battery systems. *IEEE Trans. Energy Convers.* **2011**, *26*, 737–743.
9. Xiong, R.; He, H.; Sun, F.; Zhao, K. Online estimation of peak power capability of li-ion batteries in electric vehicles by a hardware-in-loop approach. *Energies* **2012**, *5*, 1455–1469.
10. Wang, S.; Verbrugge, M.; Wang, J.S.; Liu, P. Power prediction from a battery state estimator that incorporates diffusion resistance. *J. Power Sources* **2012**, *214*, 399–406.
11. Schmidt, A.P.; Bitzer, M.; Imre, Á.W.; Guzzella, L. Model-based distinction and quantification of capacity loss and rate capability fade in Li-ion batteries. *J. Power Sources* **2010**, *195*, 7634–7638.
12. Prasad, G.K.; Rahn, C.D. Model based identification of aging parameters in lithium ion batteries. *J. Power Sources* **2013**, *232*, 79–85.
13. Samadi, M.F.; Alavi, S.M.M.; Saif, M. Online state and parameter estimation of the Li-ion battery in a bayesian framework. In Proceedings of the American Control Conference (ACC), Washington DC, USA, 17–19 June 2013; pp. 4693–4698.
14. Pop, V.; Bergveld, H.J.; Danilov, D.; Notten, P.P.H.; Regtien, P.P.L. Adaptive state-of-charge indication system for Li-ion battery-powered devices. *World Electr. Veh. J.* **2007**, *1*, 38–45.
15. Pop, V.; Bergveld, H.J.; Notten, P.H.L.; Op het Veld, J.H.G.; Regtien, P.P.L. Accuracy analysis of the state-of-charge and remaining run-time determination for lithium-ion batteries. *Measurement* **2009**, *42*, 1131–1138.
16. Tang, X.; Mao, X.; Lin, J.; Koch, B. Capacity estimation for Li-ion batteries. In Proceedings of the American Control Conference (ACC), San Francisco, CA, USA, 29 June–1 July 2011.
17. Dubarry, M.; Svoboda, V.; Hwu, R.; Liaw, B.Y. Incremental capacity analysis and close-to-equilibrium OCV measurements to quantify capacity fade in commercial rechargeable lithium batteries. *Electrochem. Solid-State Lett.* **2006**, *9*, A454–A457.
18. Zheng, Y.; Lu, L.; Han, X.; Li, J.; Ouyang, M. LiFePO₄ battery pack capacity estimation for electric vehicles based on charging cell voltage curve transformation. *J. Power Sources* **2013**, *226*, 33–41.
19. Bloom, I.; Jansen, A.N.; Abraham, D.P.; Knuth, J.; Jones, S.A.; Battaglia, V.S.; Henriksen, G.L. Differential voltage analyses of high-power, lithium-ion cells 1. Technique and application. *J. Power Sources* **2005**, *139*, 295–303.

20. Weng, C.; Cui, Y.; Sun, J.; Peng, H. On-board state of health monitoring of lithium-ion batteries using incremental capacity analysis with support vector regression *J. Power Sources* **2013**, *235*, 36–44.
21. Chen, Z.; Mi, C.C.; Fu, Y.; Xu, J.; Gong, X. Online battery state of health estimation based on genetic algorithm for electric and hybrid vehicle applications. *J. Power Sources* **2013**, *240*, 184–192.
22. Dubarry, M.; Truchot, C.; Liaw, B.Y.; Gering, K.; Sazhin, S.; Jamison, D.; Michelbacher, C. Evaluation of commercial lithium-ion cells based on composite positive electrode for plug-in hybrid electric vehicle applications. Part II. Degradation mechanism under 2 C cycle aging. *J. Power Sources* **2011**, *196*, 10336–10343.
23. Verma, P.; Maire, P.; Novák, P. A review of the features and analyses of the solid electrolyte interphase in Li-ion batteries. *Electrochimica Acta* **2010**, *55*, 6332–6341.
24. Aurbach, D. Review of selected electrode-solution interactions which determine the performance of Li and Li ion batteries. *J. Power Sources* **2000**, *89*, 206–218.
25. Pinson, M.B.; Bazant, M.Z. Theory of SEI formation in rechargeable batteries: Capacity fade, accelerated aging and lifetime prediction. *J. Electrochem. Soc.* **2012**, *160*, A243–A250.
26. Safari, M.; Morcrette, M.; Teysot, A.; Delacourt, C. Multimodal physics-based aging model for life prediction of Li-ion batteries. *J. Electrochem. Soc.* **2008**, *156*, A145–A153.
27. Peled, E.; Golodnitsky, D.; Ardel, G. Advanced model for solid electrolyte interphase electrodes in liquid and polymer electrolytes. *J. Electrochem. Soc.* **1997**, *144*, L208–L208.
28. Yoon, S.; Hwang, I.; Lee, C.W.; Ko, H.S.; Han, K.H. Power capability analysis in lithium ion batteries using electrochemical impedance spectroscopy. *J. Electroanal. Chem.* **2011**, *655*, 32–38.
29. Li, X.; Wang, T.; Pei, L.; Zhu, C.; Xu, B. A comparative study of sorting methods for lithium-ion batteries. In Proceedings of the Transportation Electrification Asia-Pacific (ITEC Asia-Pacific), 2014 IEEE Conference and Expo, Beijing, China, 31 August–3 September 2014; pp 1–6.
30. Waag, W.; Käbitz, S.; Sauer, D.U. Experimental investigation of the lithium-ion battery impedance characteristic at various conditions and aging states and its influence on the application. *Appl. Energy* **2013**, *102*, 885–897.
31. Hu, X.; Li, S.; Peng, H. A comparative study of equivalent circuit models for Li-ion batteries. *J. Power Sources* **2012**, *198*, 359–367.
32. He, H.; Xiong, R.; Guo, H.; Li, S. Comparison study on the battery models used for the energy management of batteries in electric vehicles. *Energy Convers. Manag.* **2012**, *64*, 113–121.
33. Wang, S.; Verbrugge, M.; Wang, J.S.; Liu, P. Multi-parameter battery state estimator based on the adaptive and direct solution of the governing differential equations. *J. Power Sources* **2011**, *196*, 8735–8741.
34. Ljung, L. *System Identification: Theory for the User*, 2nd ed.; Prentice Hall: Englewood Cliffs, NJ, USA, 1999.
35. Verbrugge, M.; Koch, B. Generalized recursive algorithm for adaptive multiparameter regression application to lead acid, nickel metal hydride, and lithium-ion batteries. *J. Electrochem. Soc.* **2006**, *153*, A187–A201.